Chemical Engineering Science 195 (2019) 519–530

Contents lists available at ScienceDirect

Chemical Engineering Science

journal homepage: www.elsevier.com/locate/ces

Tortuosity and connectivity evaluation by CFD simulation for morphological characterization of membranes and catalytic structures. Case study: CaF_2-like structure

Giulia Azzato [a], Giuseppe De Marco [b], Virgilio Stellato [a], Yu Sun [c,d], Alessio Caravella [a,*]

[a] Department of Environmental and Chemical Engineering (DIATIC), University of Calabria, Via P. Bucci, Cubo 44A, Rende, CS 87036, Italy
[b] Information Technology Center (ICT), University of Calabria, Via P. Bucci, Cubo 22B, Rende, CS 87036, Italy
[c] Institute for International Collaboration, Hokkaido University, Sapporo, Hokkaido 060-0815, Japan
[d] Department of Chemistry, Faculty of Science, Hokkaido University, N10W8, Kita-ku, Sapporo, Hokkaido 060-0810, Japan

HIGHLIGHTS

- A CFD-based approach for morphological characterisation of porous structures is presented.
- The CaF_2 structure is completely characterised in terms of tortuosity and connectivity.
- A *Morphology Map* is developed to show the connection status of the structure.
- The concept of Minimum Connection Curve is introduced.
- Tortuosity and connectivity are shown to be highly correlated with the *effective porosity*.

GRAPHICAL ABSTRACT

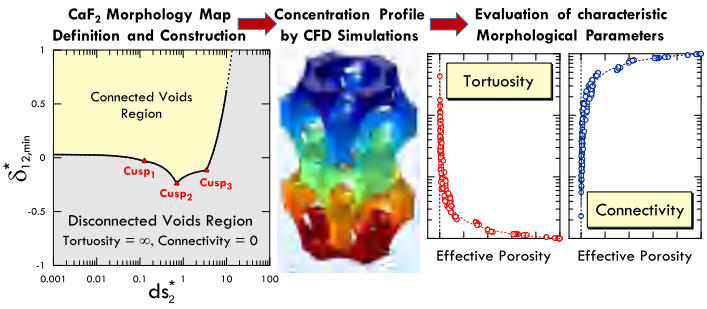

ARTICLE INFO

Article history:
Received 10 July 2018
Received in revised form 31 August 2018
Accepted 29 September 2018
Available online 29 September 2018

Keywords:
Connectivity
Tortuosity
Morphology map
CaF_2 structure
Connection curve
Porous media

ABSTRACT

A systematic methodology to characterise porous structure of membranes and catalysts in terms of tortuosity and connectivity is presented. The considered case study is the CaF_2-like structure of bidisperse spherical particles (i.e., inner and outer particles with different diameters), which are allowed to overlap. Consequently, the morphology of the resulting structure is shown to be completely determined by two geometrical parameters (two degrees of freedom). For this investigation, a *Morphology Map* is developed, it being a plot mapping void connection as a function of the characteristic geometrical parameters. Within such a map, we introduce the so-called *Minimum Connection Curve*, which is a characteristic curve representing the boundary between the connected region and the disconnected one (zero connectivity). It is then found that the CaF_2-like structure has three specific points where there is an abrupt change in the morphology behaviour, also correlated to the normalised surface area. Then, the structure tortuosity and connectivity are systematically evaluated in a wide range of geometrical conditions of the two parameters characterising the considered structure. As a result, it is shown that it is not possible to express these parameters as a unique function of porosity. However, both tortuosity and connectivity are found to be correlated with a good approximation in a certain range of porosity values with a geometrical parameter that we called *Effective Porosity*, which is the porosity available for diffusion at the minimum connection conditions. Convenient empirical correlations are eventually provided to allow readers to evaluate tortuosity and connectivity in a wide range of values.

* Corresponding author.
E-mail address: alessio.caravella@unical.it (A. Caravella).

https://doi.org/10.1016/j.ces.2018.09.051
0009-2509/

Nomenclature

Symbols

a	normalised surface area, –
C	molar concentration, mol m^{-3}
c_1, c_2	fitting parameters in Eq. (9)
D	diffusion coefficient, m^2 s^{-1}
d_{s1}	FCC particle diameter, –
d_{s2}	SC particle diameter, –
d^*_{s2}	dimensionless SC particle diameter, –
J	molar flux, mol s^{-1} m^{-2}
L	length of the unit cell edge, m
R^2	determination coefficient
V	volume, m^3
w	mass fraction, –
z	axial abscissa, m

Greek symbols

δ_{12}	Surface-Surface distance between the nearest SC and FCC particles
δ^*_{12}	dimensionless Surface-Surface distance between the nearest SC and FCC particles
ε	porosity, –
φ	connectivity factor, –
τ	diffusional tortuosity, –

Subscripts & superscripts

'1'	referred to FCC particles
'2'	referred to SC particles
a, b	abscissae in the unit cell stack where high and low concentration are set
Eff	effective (Porosity or Diffusivity)
i, j	generic i^{th} and j^{th} species
Min	minimum (Connection)

Acronyms

FCC	Face-Centred Cubic
SC	Simple Cubic

1. Introduction

With the tremendous enhancement in fabrication of innovative and more performing catalytic structures, membranes and hierarchical porous media, the importance of a more precise characterisation of porous structures has become progressively more important. The usual first characterization of a structure is made by techniques like X-ray Diffraction (XRD), Scanning Electron Microscopy (SEM), Field-emission Scanning Electron microscopy (FESEM), Transmission Electron Microscopy (TEM) and Infra-Red spectroscopy (IR), Dynamic Light Scattering (DLS) and Energy-Dispersive X-ray spectroscopy (EDX), which provide important information about morphology, crystallinity degree, defects, etc.

However, for some applications like catalysis, sorption and/or membrane-assisted reaction/separation processes, such information can be not enough for a precise understanding of the structure role in processes to which they are applied. These considerations assume a particular importance if considering that a structure can change its morphology due to kinetic and transport phenomena.

As an instance, during growth, a crystal structure is subject to severe morphological changes, which the physical, mechanical, catalytic, adsorption and optical properties depend on (Sunagawa, 1999). Other examples are (i) sintering owing to high-temperature or nucleation processes, where there is a merging and/or a spatial redistribution of surface areas and volumes to form new shapes of different morphological properties (Gao et al., 2012), and (ii) the so-called *breathing* phenomenon occurring in some complex coordination particles like MOFs, where the structure accomplishes the presence of external molecules by changing its conformation (Schneemann et al., 2014). Therefore, in most cases, a different and more transport phenomena-oriented characterisation is required for porous media.

Among several morphological parameters of interest, tortuosity is one of the most investigated properties. Although this parameter is often considered as a fitting parameter to calculate by means of non-linear regression and a number of empirical correlations with porosity have been developed (Pisani, 2011), nevertheless it actually has a specific physical meaning related to the structure morphology, providing crucial information about catalytic and hierarchical porous structures (Zalc et al., 2004; Caravella et al., 2012, 2016; Delarue and Jeulin, 2003; Coleman and Vassilicos, 2008; Wiedenmann et al., 2013; Moh'd, 2015; Landesfeind et al., 2016) as well as biological systems for diagnosis purpose (Herremans et al., 2015; Grisan et al., 2008; Maude et al., 2014; Muraoka et al., 2014; Sasongko et al., 2015; Annunziata et al., 2016).

The importance of tortuosity is stated by the number of papers focusing on its evaluation carried out by means of different techniques involving computational fluid dynamics (Shen and Chen, 2007; Caravella et al., 2012; Anovitz and Cole, 2015; Kong et al., 2015; Bellini et al., 2018), lattice-Boltzmann (Matyka et al., 2008; Duda et al., 2011; Wang and Boltzmann, 2014; Espinoza et al., 2015) and Monte-Carlo simulations (Kim and Chen, 2006) implemented on digitally-reconstructed models by computer-aided tomography and other image reconstruction algorithms (Alam et al., 2006; Promentilla and Sugiyama, 2007; Yamashita et al., 2009; Gommes et al., 2009; Vallavh, 2009; Rezanezhad et al., 2009; Szczepanski et al., 2010; Sobieski et al., 2012; Solórzano et al., 2013; Manickam et al., 2014; Chen-Wiegart et al., 2014; Berg, 2014; Ranachowski et al., 2015; Khabbazi, 2015; Farlenkov, 2015; Pawlowski et al., 2018). However, considering that the definition itself of tortuosity is not unique, its evaluation and related experimental methodologies are not an easy task to face (see, e.g., (Vogel, 1997; Vogel and Roth, 1998; Moreau et al., 1999; Moldrup et al., 2001; Promentilla et al., 2009; Lichtner et al., 2015; Melo, 2005; Le et al., 2010; Nwaizu and Zhang, 2015). Specifically, the majority of literature papers are for the most focused on (i) diffusional tortuosity (Kim and Chen, 2006; Ranachowski et al., 2015; Promentilla and Sugiyama, 2007; Yamashita et al., 2009; Gommes et al., 2009; Manickam et al., 2014; Chen-Wiegart et al., 2014) and (ii) hydraulic tortuosity (Herremans et al., 2015; Alam et al., 2006; Berg, 2014; Matyka et al., 2008; Duda et al., 2011; Wang and Boltzmann, 2014; Vallavh, 2009; Rezanezhad et al., 2009; Szczepanski et al., 2010; Sobieski et al., 2012), which are defined based on effective diffusivity and hydraulic permeability, respectively. These different definitions put in evidence an important aspect: the type of tortuosity is determined by the particular transport phenomenon with respect to which it is evaluated.

Remarkable examples of such a concept can be found in Yamashita et al. (Yamashita et al., 2009), where tortuosity is defined to measure the quantity of sound waves through the material voids

(Yamashita et al., 2009), and in Brun et al. (2008), where tortuosity is defined through the heat transfer (Brun et al., 2008). In the former, acoustic impedance measurements obtained from absorption tests are used, whereas conductivity measurements are carried out in the latter. Such tortuosity types are evidently different from both the diffusive and the hydraulic one, as the transport of sound waves as well as the transport of heat transfer, which in general are able to "permeate" the solid walls of the porous media, acts differently from mass diffusion and convection. Since in our investigation we want to characterise the voids morphology in terms of geometrical parameters, we have chosen to consider the diffusional tortuosity, which has been already demonstrated to be a function of geometrical properties only (Whitaker, 1977; Kim et al., 1987; Quintard, 1993; Quintard and Whitaker, 1993; Ciesko, 2009; Guo, 2012).

An important aspect to be underlined is that the diffusional tortuosity is a scale-independent parameter and can be used to calculate the effective diffusion coefficient in whatever diffusion regime. In fact, even when the length scale is such that the molecule size is comparable with the pore size, the diffusional tortuosity should be used to correct the unconstrained (straight) diffusional paths to match the actual pore path. The additional direction changes of a diffusing molecule due to the impact with the pore walls do not depend on geometry only and have to be considered in appropriate transport models. Examples of this fact are (i) the Knudsen diffusion model, whose diffusivity should be corrected with the pore tortuosity even if already includes the mean constrained path of the molecules, and (ii) the transport model through zeolite membranes developed more recently in Caravella et al. (2016), where a correction to the diffusional tortuosity of zeolite is introduced to include the influence of species adsorbed on the pore walls (Caravella et al., 2016).

Concerning connectivity, no standard definition exists in the literature and, thus, the few papers measuring/evaluating this parameter use different approaches (Bellini et al., 2018; Promentilla et al., 2009; Lichtner et al., 2015; Vogel, 1997; Vogel and Roth, 1998; Moreau et al., 1999). In particular, Vogel (1997) and Vogel and Roth (1998), used the Euler-Poincare characteristic to quantify connectivity, whereas Moreau et al. (1999) measured it by the propagation method. Later, Promentilla et al. (2009) and, subsequently, Lichtner et al. (2015) used surface reconstruction techniques considering the number of connected voxels with respect to standalone ones. However, those methodologies are not applicable where a digital version of the structure is not available.

More recently, our research group published a paper where a direct relation between diffusional tortuosity and connectivity is stated, defining the latter as the inverse of the former (Eq. (1)) (Bellini et al., 2018). Consequently, the connectivity factor defined in Eq. (1) measures the degree of *diffusional connectivity*, which is a geometrical property by definition.

$$\begin{aligned} &Connectivity\ Factor\ \phi \equiv \tfrac{1}{Tortuosity\ \tau} \\ &Limits: \begin{cases} \phi \to 0 \iff \tau \to \infty \\ \phi = 1 \iff \tau = 1 \end{cases} \end{aligned} \tag{1}$$

Eq. (1) is based on the consideration that the structure voids are poorly linked to each other in porous media with a high tortuosity value.

This situation is briefly sketched in Fig. 1, which depicts a sketch of different connection conditions in relation with tortuosity. In particular, the definition reported in Eq. (1) incorporates the concept that a porous structure having all voids that are non-accessible (i.e., completely disconnected, Fig. 1c) must have a zero connectivity, whose value should increase as voids become progressively more connected to each other (Fig. 1a and b). From a physical point of view, this means that there are inner voids that do not contribute to the transport phenomenon considered for characterization (ordinary diffusion in this case). In practise, if a hypothetical molecule were placed inside an isolated void, it would remain entrapped in that void without being able to escape (dashed closed paths in Fig. 1b and c).

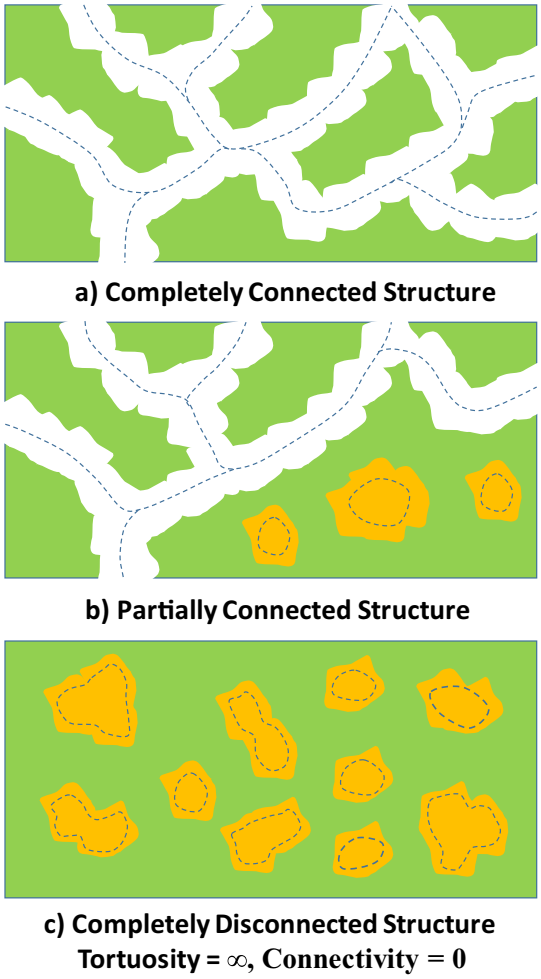

Fig. 1. General sketch of different connection situations. The disconnected voids are highlighted in dark yellow. The dashed lines are the schematic representation of average diffusional paths. (For interpretation of the references to color in this figure legend, the reader is referred to the web version of this article.)

In this context, the aim of our paper is to provide a general methodology to characterise structures in terms of diffusional tortuosity and connectivity degree evaluated by computational fluid dynamic techniques. For this purpose, the CaF_2-like structure is chosen as a case study, even though the proposed methodology can be applied as well to every regular and irregular structures provided the availability of appropriate representative three-dimensional models.

The considered CaF_2-like structure is involved in important when hydrogen atoms form hydrides within FCC metals like palladium. In fact, at relatively low energy levels (lower H-concentration in the lattice) the H-atoms preferentially occupy the octahedral sites within the original FCC unit cell, whose configuration corresponds to the NaCl-like structure. However, at a sufficiently high-energy level (high H-concentration in the lattice) the H-atoms prefer to occupy the tetrahedral sites, thus leading to a CaF_2 atomic structure (Fukai, 1984). The latter situation corresponds to high-pressure conditions, which are of interests for industrial application in hydrogen purification and/or storage.

Therefore, the need of fundamental understanding of the hydrides structural morphology assumes a crucial importance. To the best of the Authors' knowledge, the study presented in this paper is the first example of complete and systematic characterization of the CaF_2 structure in terms of tortuosity and connectivity, showing that even apparently simple structures can hide interesting and intriguing aspects, which have to be studied in a more detail with the objective to withdraw information to better understand the behaviour of more complex structures. The following sections provide the details of our analysis.

2. Description of the system

The CaF_2 structure is composed of a Face-Centred Cubic (FCC) structure containing a Simple Cubic (SC) structure whose vertices are placed at the centres of the FCC inner tetrahedral sites (blue particles, Fig. 2a). In this study, we consider spherical particles with two different diameters for the outer FCC structure and inner SC one, respectively. Therefore, once the two particle diameters and a length of another geometrical entity like the surface-surface distance between the closest SC and FCC particles are set (as done in the present investigation), the structure can be univocally built (Table 1). However, the length of a particle diameter is just needed to set the scale of the actual geometry. Accordingly, once the scale is set, the geometry depends just on the two dimensionless geometrical parameters (bidisperse structure) reported in Table 2, where the diameter of the FCC particles is chosen as the reference length with respect to which to normalise the others. The choice to work with dimensionless parameters assures that the obtained results are scale-independent, which is in line with the fact that the morphological properties of a structure (like porosity, tortuosity and connectivity) must not depend on the particular scale chosen.

In order to analyse in detail the morphology changes as a function of the spatial distribution of the exposed particle surface, the values of d^*_{s2} and δ^*_{12} are let vary to allow the investigation of both non-overlapping and overlapping structures. With this choice, the edge of the unit cell L is expressed as a function of the characteristic geometrical parameters as follows (Eq. (2)):

$$L = \frac{2}{3}\sqrt{3}d_{s1}(2\delta^*_{12} + d^*_{s2} + 1) \tag{2}$$

Table 1
Geometrical parameters set to build the CaF2 structures.

Parameter	Description	Units
$\boldsymbol{d_{s1}}$	Diameter of the outer FCC particles	[m]
$\boldsymbol{d_{s2}}$	Diameter of the inner SC particles	[m]
$\boldsymbol{\delta_{s2}}$	Surface- Surface interparticle distance between two closest FCC and SC particles	[m]

Table 2
Dimensionless geometrical parameters related to the degrees of freedom of the CaF_2 Structure.

Parameter	Definition	Description
$\boldsymbol{d^*_{s2}}$	d_{s2}/d_{s1}	Dimensionless diameter of the inner SC particles
$\boldsymbol{\delta^*_{12}}$	δ_{12}/d_{s1}	Dimensionless interparticle distance

As well, porosity does also depend on these two parameters, even though that functionality is too complex to be expressed analytically in the case of overlapping particles. This aspect is remarked since a plenty of papers in the literature attempt to find convenient relationships between tortuosity and porosity (Pisani, 2011), which however is not possible in general. That can be done just in some specific cases, like for monodisperse structures of spherical particles (Caravella et al., 2012), in the limit of unitary porosity (Maxwell, 1881) and for an infinitely-disperse swarm of particles (Neale and Nader, 1973). For what said before, in the present case there cannot be a bijective relationship between porosity and tortuosity, as shown later in Section 4. To highlight the complexity of the investigated structures, Fig. 3 shows some examples of possible configurations, where the visualised volume represents the void space available for diffusion. As shown later, these structures can be considered to belong to four different morphological families, which are identified by a morphology map, as described in detail in Section 4.1.

3. Simulation settings

3.1. Computational fluid dynamic approach

As mentioned above, tortuosity is evaluated by solving the pure diffusion problem within the considered porous structures using a

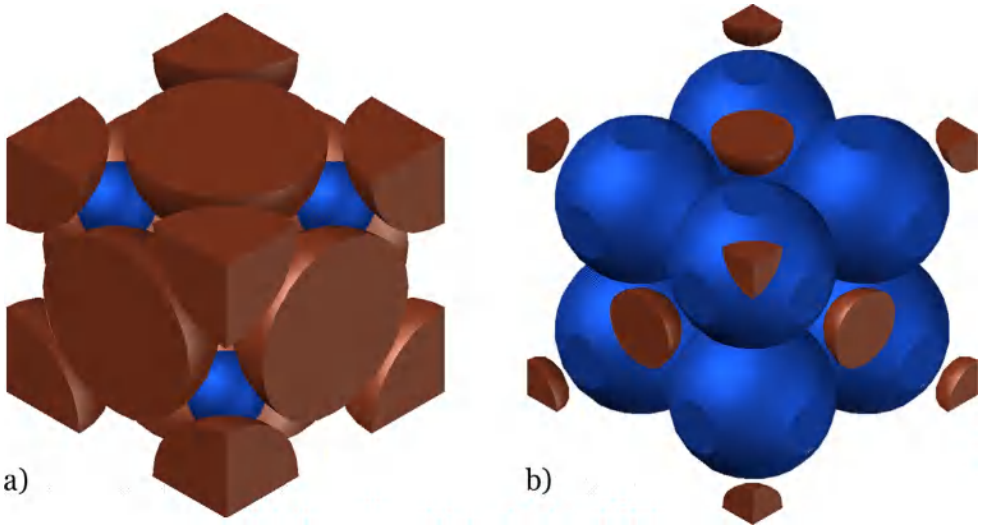

Fig. 2. Examples of unit cells relative to CaF_2-like structures of spherical particles displayed in two general cases: Internal SC-structured particles (a) smaller and (b) larger than the FCC-structured ones.

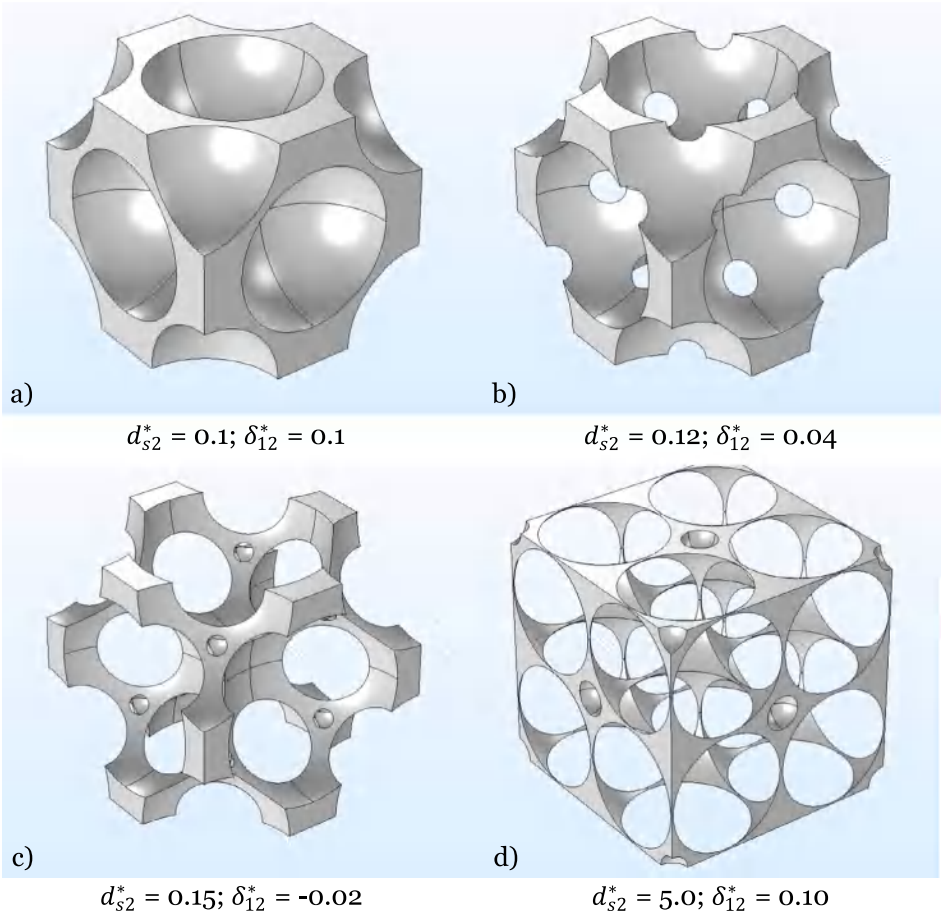

Fig. 3. Examples of unit cells investigated for certain values of d^*_{s2} and δ^*_{12}.

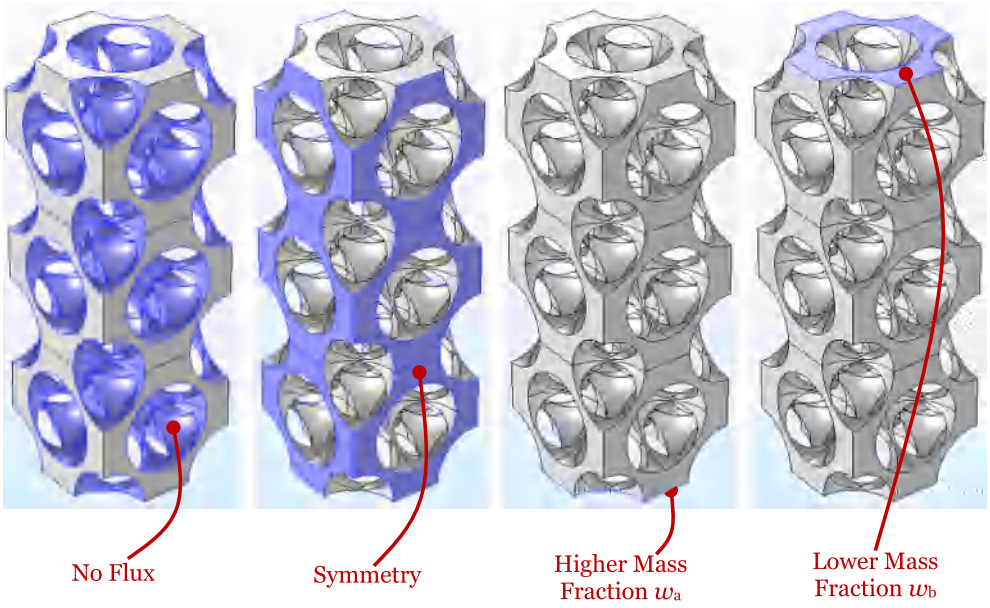

Fig. 4. Boundary conditions set for simulation. The considered structure example corresponds to d^*_{s2} = 0.75; δ^*_{12} = −0.20, which is shown for convenience of the readers.

computational fluid dynamics-based methodology. The pure diffusion problem is implemented through Fick's law (Eq. (3)), which is used as the constitutive equation for the molar flux of a homogeneous binary gas mixture inter-diffusing within the structure voids:

$$J_i = -D_{ij}\underline{\nabla}C_i \tag{3}$$

where D_{ij} is the free diffusivity in a fluid without obstacles and $\underline{\nabla}C_i$ is the concentration gradient. It is important to remark that the diffusional tortuosity is a geometrical property and, thus, its value

does not depend on the particular methodology used here for its evaluation.

Simulations are performed using the software COMSOL MULTIPHYSICS®, which provides the average diffusive flux between the two faces where the two concentration values are set. From such information, the effective diffusivity is calculated as follows (Eq. (4)) (Caravella et al., 2012; Bellini et al., 2018):

$$D_{ij,Eff} = -\frac{J_i \Delta z}{\Delta C_i} \times \frac{A_{Void}}{A_{Total}} \tag{4}$$

where ΔC_i, Δz, A_{void} and A_{Total} indicate concentration difference, distance between the faces where high and low concentrations are set, cross-sectional area available for diffusion (i.e., void area) and the total one (i.e., the nominal square area of a cell face). Then, tortuosity is calculated as follows:

$$\tau = \varepsilon \frac{D_{ij}}{D_{ij,Eff}} \tag{5}$$

Table 3
Simulation Parameters.

Parameter	Description	Value
w_a	Higher mass fraction	$2 \cdot 10^{-4}$ mol m^{-3}
w_b	Lower mass fraction	$1 \cdot 10^{-4}$ mol m^{-3}
D_{ij}	Binary diffusion coefficient	$1 \cdot 10^{-7}$ m^2 s^{-1}

Table 4
Parameters of mesh-independency analysis.

Parameter	Finer mesh	Coarser mesh	Units
d^*_{s2}	0.5		[–]
δ^*_{12}	−0.11		[–]
Maximum element growth rate	2	1.5	[–]
Curvature factor	0.06	0.1	[–]
Resolution of narrow region	1.33	1	[–]
Tortuosity τ	*Finer mesh*	*Coarser mesh*	*Difference*
	2.32805	2.32341	0.2%

As for the Connectivity Factor φ, it is evaluated as the inverse of tortuosity, as indicated in Eq. (1). To minimise the computational errors owing to possible perturbations in the diffusion streamlines, assemblies of two or three unit cells are used in all simulations.

Fig. 4 shows an example of built assemblies along with the boundary conditions set for simulation, for which the impenetrability of the particle walls (no flux) is set together with symmetry on the flat lateral boundaries of the cell stacks and concentration values on the respective bases (see Table 3).

3.2. Mesh settings

The computational mesh required for simulation is generated using the settings shown in Table 4, reporting the key-parameters characterising the meshing process. In order to assure that the obtained results are independent of the mesh type, we have preliminarily set two simulations at the same operating conditions but with different meshing parameters, corresponding to a finer and a coarser mesh, respectively. The former has at least eight elements filling the shortest surface-surface distance in the structure (Fig. 5a), whereas the latter has four elements (Fig. 5b). As a result, the difference of the so-calculated tortuosity values is around 0.2%, which is an acceptable tolerance for our purpose. Anyway, to be conservative, we have applied the criterion of the eight elements (finer mesh) to the meshes built in all simulations.

4. Results and discussion

4.1. Morphology map

In Fig. 6a, we present the here-defined *Morphology Map* of the considered structure, which is built in terms of minimum value of δ^*_{12} (here indicated with $\delta^*_{12,min}$) vs. d^*_{s2}. This plot arises from the consideration that, as mentioned above, the morphology of a bidisperse structure of spherical particles has two degrees of freedom. Therefore, if we fix the value of one parameter letting the

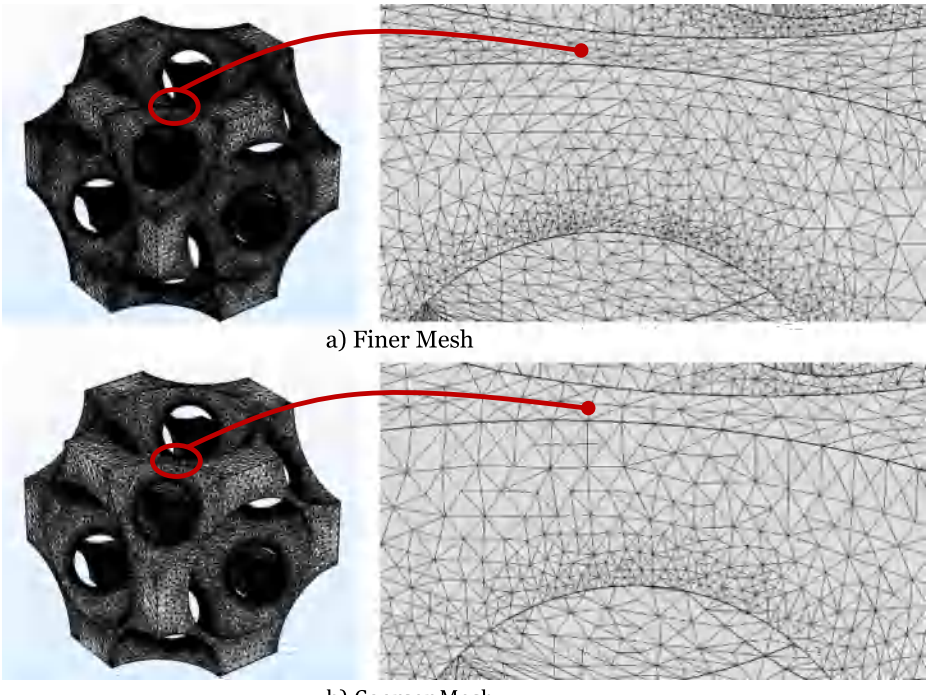

Fig. 5. Sensitivity of tortuosity to mesh. Porosity = 0.2474.

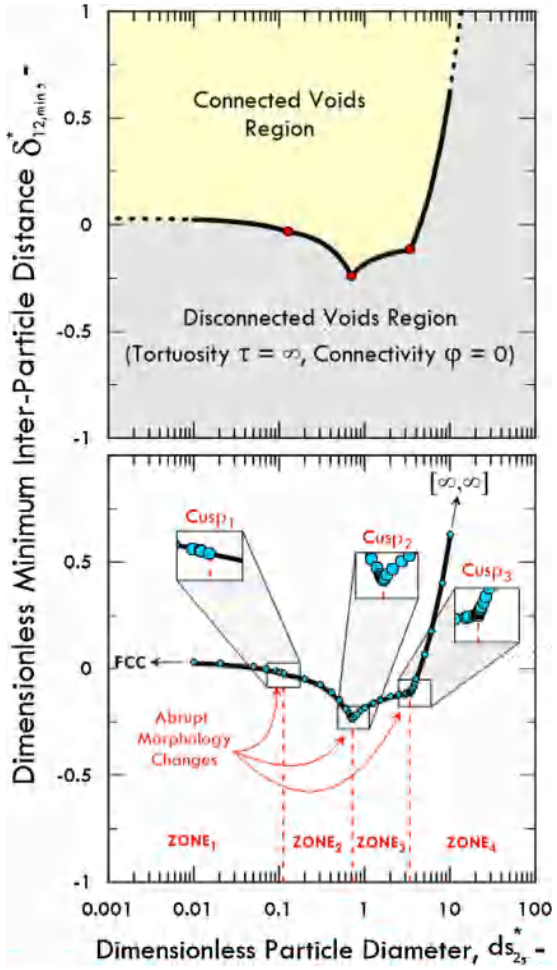

Fig. 6. Morphological map of the CaF_2-like structure. The figures is split into two parts for a better readability.

other one vary within a sufficiently wide range of values, we obtain a continuous curve. We remark that this is generally valid for whatever bidisperse structure, thus being not limited to the structure considered in the present work. In this specific case, each point of the curve is obtained by fixing a certain value of d^*_{s2} and evaluating the corresponding unique specific value of δ^*_{12} ($\delta^*_{12,min}$) below which the structure voids are completely disconnected in the sense reported above (Fig. 1c). Therefore, making d^*_{s2} vary over an appropriate interval of values, we obtain a curve representing the boundary between two morphological regions, whose structure is characterised by connected and completely disconnected voids, respectively. All points along the curve correspond to what will be referred to as *minimum connection conditions* throughout the present paper.

The presented map, shown here for the first time in the open literature to the best of our knowledge, is numerically obtained by an in-house user-defined function just developed for this purpose and, furthermore, is completely general and cover all the possible morphologies of CaF_2-like structures of spherical particles, whence the reason of its name. In the limit of d^*_{s2} tending to zero, the curve tends to the value of $\delta^*_{12,min}$ of the FCC structure, as the internal SC particles in practise disappear. Differently, in the opposite limit (d^*_{s2} tending to infinity), the curve tends to infinity and not to the value of the SC structure. This occurs because the presence of the outer FCC particles limiting the boundaries of the unit cell is unavoidable even if their diameter is almost null. Moreover, there exist three characteristic points of the curve, which are denoted in red and evidenced in the zoom views in Fig. 6b. As we are going to demonstrate, these points are actually *cusp* points in a mathematical sense, because the structure is subject to a more or less abrupt morphology change in their correspondence.

The demonstration of whether these points are really cusps or not is required as the curve is obtained numerically. In fact, for example, the point corresponding to the $Cusp_2$ could be a minimum with a null derivative, instead. This represents not just a merely numerical issue but rather an important morphological aspect. Let us remark that, from a mathematical point of view, a cusp is a point where a curve is continuous but not derivable; in practise, the right derivative is different from the left one.

To demonstrate that these points are cusps, we report the morphology evolution of the structure for certain values of d^*_{s2} on the *Morphology Map* (Fig. 7). As can be observed by following the structures from the picture (a) on, the position of the red circles indicating the detachment points change from (d) to (e). This indicates that the morphology behaviour before (d) and after (e) are different, thus generating the $Cusp_1$ reported in Fig. 6b. Going on along the curve, the structure morphology passes from (i) to (j), where the position of the detachment point is the same, but its shape is different, as shown in the zoomed detail. Since such shapes are quite different from each other, the consequent generated $Cusp_2$ is more pronounced than the $Cusp_1$. Finally, when the structure experiences the morphology change from (p) to (q), again the detachment point changes position, thus resulting in the $Cusp_3$. Considering that $Cusp_1$ and $Cusp_3$ are caused by different positions of detaching points, it thus means that from a physical point of view there are two detachment points at such cusps at the same time. Differently, the structure corresponding to $Cusp_2$ has the peculiarity to detach at the same point discontinuously. These aspects can be also observed in Fig. 8, where normalised surface area (a, see Eq. (6)) and porosity are evaluated as functions of d^*_{s2} at minimum connection conditions (a_{Min} and ε_{Min}, respectively). In particular, the cusps appear more evidently in the two curves, especially in that of the normalised surface area.

$$a \equiv \left.\frac{\text{Exposed Area}}{\text{Area of the Unit Cube}}\right|_{\substack{Unit\\Cell}} \tag{6}$$

Interestingly, both a_{min} and ε_{min} show trends of similar shapes, exhibiting a maximum at a value of d^*_{s2} close to the unity. This indicates that the unit cell of the CaF_2-like structure has the highest specific surface area and the highest porosity when the diameters of the outer FCC particles and the inner SC ones are equal, which corresponds to the case of a monodisperse structure. The other relative maximum is located at around d^*_{s2} equal to 0.5, corresponding to the case where the inner particles have a diameter half of the outer ones. It can be also noticed that, among all cusp points, $Cusp_2$ shows the highest porosity ε_{min}, followed by $Cusp_1$ and $Cusp_3$. The physical meaning of this behaviour can be understood by considering that a single detaching position ($Cusp_2$) generates bigger disconnected "islands", whereas in the other cases ($Cusp_1$ and $Cusp_3$) the islands are smaller. Such a concept seems to be confirmed by the fact that $Cusp_1$ shows a lower number of islands than $Cusp_3$ in the unit cell, which again favours the formation of bigger islands. As for the normalised surface area a_{min}, the order is the following: $Cusp_2 > Cusp_3 > Cusp_1$, which is slightly different from the porosity trend. In fact, also in this case $Cusp_2$ shows the highest a_{min}, but the $Cusp_3$ value overcomes the $Cusp_1$ one. The explanation for that lies in the formation of a higher number of islands for $Cusp_3$ generating a higher exposed area.

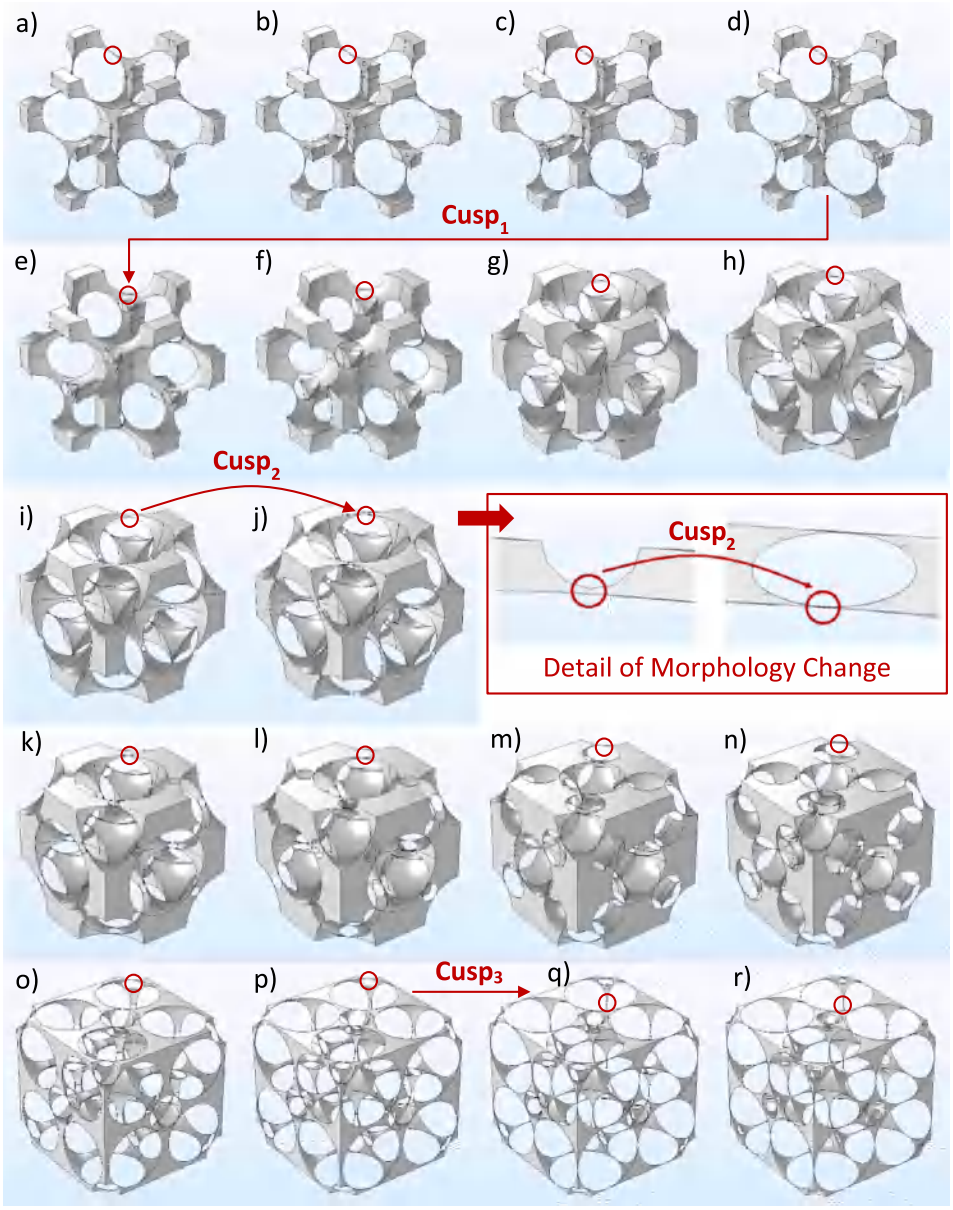

Fig. 7. Evolution of the morphology at minimum connection conditions value as a function of d^*_{s2} = {(a): 0.05, (b): 0.07, (c): 0.09, (d): 0.10, (e): 0.20, (f): 0.30, (g): 0.50, (h): 0.60, (i): 0.65, (j): 0.75, (k): 0.90, (l): 1.00, (m): 1.25, (n): 1.50, (o): 2.50, (p): 3.00, (q): 3.40, (r): 4.00}. The red circle in each scheme indicates the point of the structure at which the detachment occurs by decreasing the value of δ^*_{12}. When the position of the detachment point changes from a structure to the successive one, the corresponding cusp appears in Fig. 6. (For interpretation of the references to color in this figure legend, the reader is referred to the web version of this article.)

4.2. Tortuosity and connectivity evaluation

After investigating the CaF_2-like structure in terms of the previously presented geometrical properties, the morphological analysis is carried out by evaluating parameters more related to transport properties, i.e., tortuosity and connectivity of the structure. For this purpose, we performed simulations letting the values of d^*_{s2} and δ^*_{12} vary independently of each other. Fig. 9 shows an example of simulation results in terms of concentration profiles, from which the tortuosity values are evaluated. As the unit cell is isotropic, in this case it is not necessary to consider other directions along which to set the concentration difference, as demonstrated in Caravella et al. (2012). The tortuosity trends are depicted in Fig. 10 as a function of δ^*_{12} for different values of d^*_{s2}. Looking at the behaviour of the single curves, we can observe that all trends tend to the maximum porosity value ($\varepsilon \to 1$) for increasing δ^*_{12}, which corresponds to a situation where the inter-particle distance becomes gradually larger. Differently, they tend to infinity as δ^*_{12} approaches the minimum connection value ($\delta^*_{12} \to \delta^*_{12,min}$), at which there are no voids connected to each other (see Fig. 1c).

To show the functionality of tortuosity with d^*_{s2}, Fig. 10 is split into two different plots (Fig. 10a and b), which show the trends corresponding to values of d^*_{s2} lower and higher than $Cusp_2$ (0.72 *ca.*), respectively. As we can observe, the tortuosity behaviour before $Cusp_2$ is different from that after it. In fact, in the former case tortuosity increases with decreasing d^*_{s2} , whereas in the latter the opposite trend is observed, which means that tortuosity shows a minimum with d^*_{s2}. It is interesting to notice that the other two cusps ($Cusp_1$ and $Cusp_3$) do not provide such a peculiarity, which is explained by considering that $Cusp_2$ is the only one among the others that is a local minimum in the morphology map depicted in Fig. 7. Overall, we can observe that all the trends are clearly

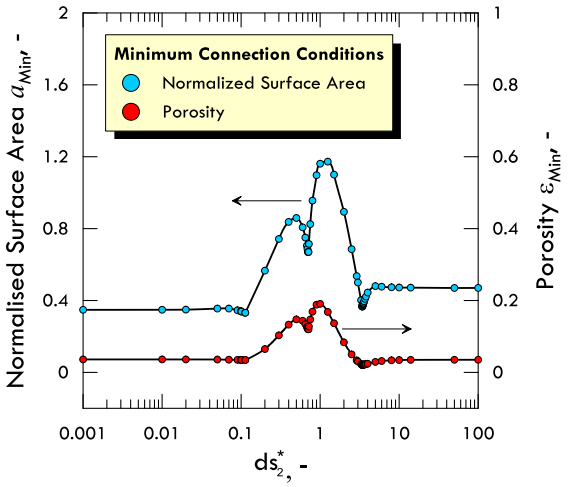

Fig. 8. Normalised surface area and porosity as functions of d^*_{s2} evaluated at minimum connection conditions.

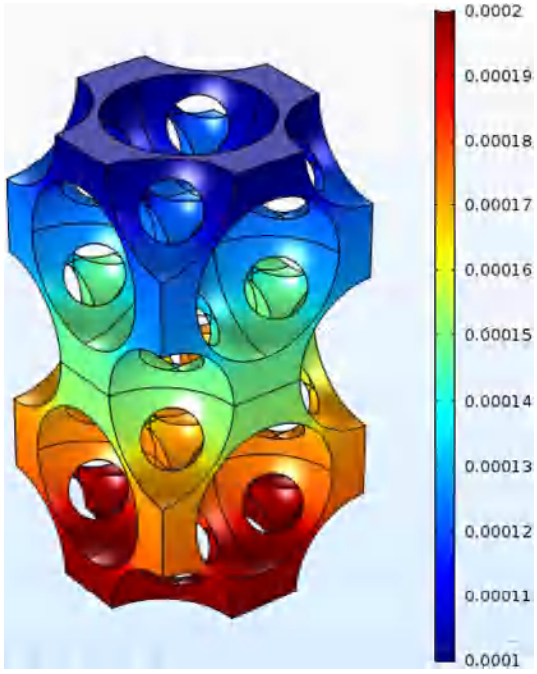

Fig. 9. Example of simulation results in terms of concentration profiles in a stack of two unit cells.

recognisable and do not intersect each other, which means that tortuosity cannot be univocally expressed as a function of just a single geometrical parameter. We remark this aspect because a number of literature works aim to correlate tortuosity with a single geometrical parameter like porosity. However, this cannot be generally done unless for particular structures, such as: (a) monodisperse structures of spherical particles (Kim and Chen, 2006; Caravella et al., 2012), (b) structures in the high-porosity limit (Maxwell, 1881) and (c) and infinitely-disperse structures (Neale and Nader, 1973).

This is evidenced in Fig. 11, where tortuosity is shown as a function of porosity along with the connectivity factor (Eq. (1)). The apparent irregularity of these plots is because porosity is itself function of d^*_{s2} and δ^*_{12}. In practise, the same tortuosity values previously reported in Fig. 10 are here shown in Fig. 11a. However, although tortuosity and connectivity cannot be univocally determined from just porosity in the whole porosity range, we found that this can be done with a very good approximation within a porosity range of 0.47–1, where Neale and Nader's model (Neale and Nader, 1973), which is formally coincident with Maxwell's one (Maxwell, 1881), is able to predict relatively well tortuosity and connectivity values within a maximum error of around 1.5%. Furthermore, from the trend depicted in Fig. 11, it can be observed that Neale and Nader's model represents the lower bound for tortuosity and, thus, the upper bound for connectivity. This fact represents an interesting aspect, as an infinitely-disperse swarm of particles has the characteristic of decreasing its porosity by keeping a completely connected structure (Fig. 1a). In practice, that ideal structure can be thought to be composed of progressively smaller particles filling the voids between the bigger particles. In such a virtual filling process, the structure porosity can gradually decrease tending to zero meanwhile keeping void inter-particle space available for diffusion. This is the physical reason why Neale and Nader's virtual structure shows the highest connectivity value and the lowest tortuosity.

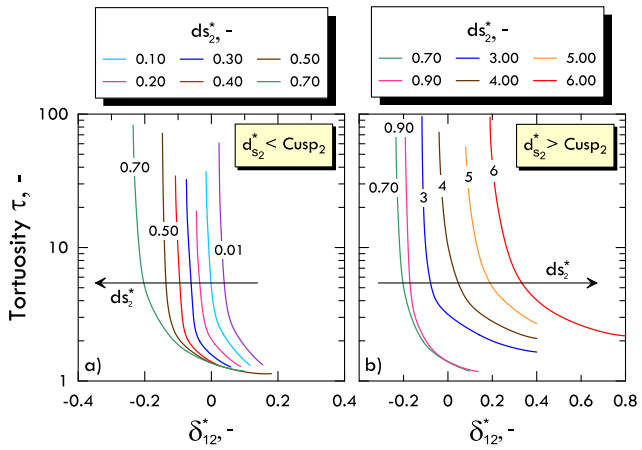

Fig. 10. Tortuosity as a function of δ^*_{12} for different values of d^*_{s2}. The curves are split into two different plots for a better readability.

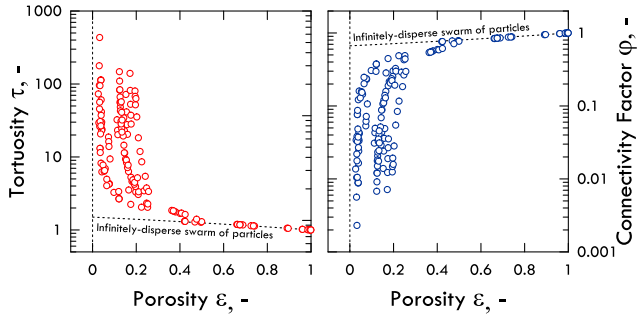

Fig. 11. Tortuosity and Connectivity Factor as functions of porosity for all the cases considered in this work. The ideal analytical trend corresponding to the case of infinitely-disperse swarm of particles developed by Neale and Nader (1973).

4.3. Empirical correlations of tortuosity and connectivity with porosity

With the aim to try to find a satisfactory correlation between tortuosity/connectivity values and a single geometrical parameter, we define the here-called *effective porosity* (ε_{Eff}) as the subtraction of the minimum porosity from the standard porosity (Eq. (7)).

$$\varepsilon_{Eff} = \frac{V_{Void} - V_{Min}}{V_{Total}} = \varepsilon - \varepsilon_{Min} \tag{7}$$

This definition for the effective porosity as well as its use as characteristic geometrical parameter is driven by the fact that tortuosity tends to infinity for porosity tending to the minimum one. It must be pointed out that the concept of effective porosity introduced here is different from the expression introduced by Wiedenmann et al. (2013), who defined an effective diffusivity as the product of the total porosity and constrictivity factor, with the latter taking into account the bottlenecks arising from reduced channel area. However, there are some conceptual analogies between the two parameters, because also in our case the area available for diffusion becomes gradually smaller as porosity decreases up to the minimum connection conditions, where the pore constriction is maximum and there exists no path connecting the structure voids. As the structure considered here is regular, the minimum connection condition (i.e., zero-connectivity in this specific case) is reached at specific porosity values, whereas in irregular ones the bottlenecks closing the diffusional paths arise gradually depending on the particular statistical distributions of the voids. Anyway, with the definition reported in Eq. (7), it is straightforward that all tortuosity values tend to infinity as ε_{Eff} tends to zero, as briefly reported in Eq. (8).

$$\lim_{\varepsilon \to \varepsilon_{Min}} \tau = +\infty \Rightarrow \lim_{\varepsilon - \varepsilon_{Min} \to 0} \tau = +\infty \tag{8}$$

The resulting plots are shown in Fig. 12 in terms of tortuosity and connectivity factor. In this figure, the data are reported using both log-linear and log-log scales to allow visualising the situation at low values of effective porosity. An interesting aspect to notice is the higher correlation degree of tortuosity and connectivity with respect to the values reported in Fig. 11, at least within the ε_{Eff} range of (0.1–1), which corresponds to a range of interest for adsorption and catalysis application. Anyway, it can be observed that the correlation degree decreases with decreasing porosity, which means that the parameter ε_{Eff} is not adequate to describe tortuosity and connectivity factor in the whole range of values.

To attempt to obtain a simple expression by which to evaluating tortuosity and connectivity factor in a convenient range of values,

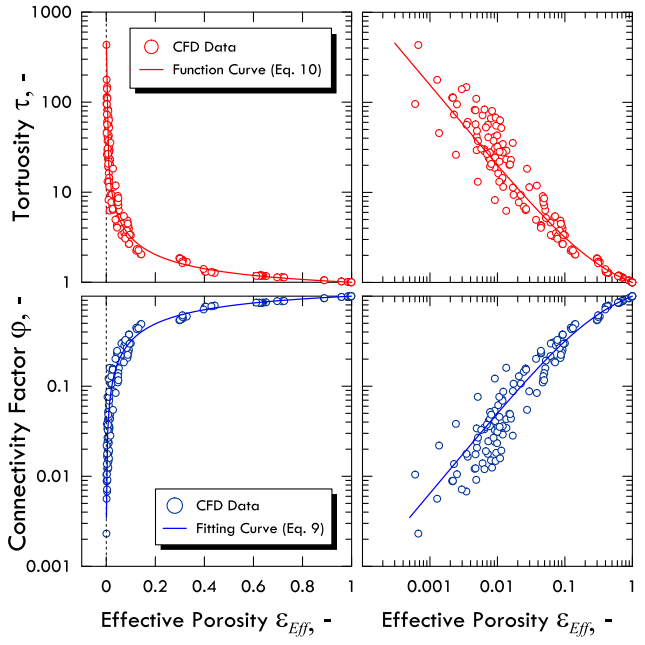

Fig. 12. Tortuosity and Connectivity Factor as functions of the effective porosity. The continuous curve in the connectivity factor plot is a fitting curve (Eq. (9)), whereas that depicted in the tortuosity plot is simply drawn as the inverse of the fitting curve (Eq. (10)).

Table 5
Fitting output based on Eq. (9) using data of connectivity factor.

Parameter	Description	Value
c_1	Fitting parameter	0.301354
c_2	Fitting parameter	0.90220
R^2	Determination coefficient	0.9862
Applicability range		$0.15 \leqslant \varepsilon_{Eff} \leqslant 1$
Maximum error		≈10%

an appropriate empirical expression for connectivity as a function of the effective porosity is proposed (Eq. (9)).

$$\begin{cases} \varphi = \dfrac{1}{1 + c_1 \dfrac{\left(1-\varepsilon_{Eff}\right)}{\varepsilon_{Eff}^{c_2}}} \\ 0.15 \leqslant \varepsilon_{Eff} \leqslant 1 \end{cases} \tag{9}$$

For this purpose, the data relative to the connectivity factor are chosen to carry out the regression procedure due to a major robustness of fitting calculation, as such a parameter is comprised within the range (0,1), whereas tortuosity does not have an upper bound (infinity). The form of such a two-parameter expression is chosen with the guideline that tortuosity, which is in fact the denominator in Eq. (9), have to tend to the unity as ε_{Eff} approaches the unity and to infinity as ε_{Eff} approaches zero. As for the curve relative to tortuosity, it is constructed by simply taking the inverse of Eq. (9) as expressed in Eq. (10), which means that no regression is carried out for tortuosity data.

$$\begin{cases} \tau = \frac{1}{\varphi} = 1 + c_1 \dfrac{\left(1-\varepsilon_{Eff}\right)}{\varepsilon_{Eff}^{c_2}} \\ 0.15 \leqslant \varepsilon_{Eff} \leqslant 1 \end{cases} \tag{10}$$

The regression results are reported in Table 5, where the satisfactory value of determination coefficient R^2 can be observed. However, although the values of the fitting parameters are calculated by regression considering the whole ε_{Eff} range, we recommend using Eq. (9) to evaluate connectivity within the ε_{Eff} range of (0.15–1), which provides a maximum error of 10%.

5. Conclusions

In this investigation, a systematic and general morphological characterisation of the CaF_2-like structure of spherical particles was carried out by computational fluid dynamics simulation. In particular, the structure behaviour was deeply analysed as a function of the two parameters that completely characterise the considered geometry (bidisperse structure), permitting particles to overlap. This allowed the number of different morphologies to be clearly identified and studied.

From such an analysis, we developed the concept of what we called *Morphology Map* of the structure, in which we introduced the *Minimum Connection Curve*, representing the locus of the points below which the internal voids are completely disconnected from each other. This map is a sort of fingerprints of the CaF_2 structure, which is found to be characterised by three characteristic abrupt morphology changes, represented by cusp points, whose existence was demonstrated by showing the morphology evolution along the minimum connection curve. The cusps were also shown in terms of porosity and normalised surface area at the same conditions.

Furthermore, analysing the behaviour of the normalised surface area, we found that there is the maximum surface area where inner (Simple Cubic) and outer (Face-Centred Cubic) particles of the structure has the same size (diameter), which corresponds to a mono-disperse structure.

Afterwards, tortuosity was calculated in a wide range of values of the two geometrical parameters characterising the considered

structure. The obtained results allowed us to show that the tortuosity of bidisperse regular structures cannot be expressed as a function of porosity only, which confirms that tortuosity is in fact an independent morphological property.

Furthermore, from the consideration that tortuosity can be thought as a measure of the difficulty for the structure voids to be connected to each other, we used the definition of connectivity factor introduced in Bellini et al. (2018) as the inverse of tortuosity to quantify the structure connectivity. Moreover, the expression valid for a swarm of infinitely-disperse particles (Neale and Nader, 1973) was confirmed to be the lower bound for tortuosity and, thus, the upper bound for connectivity.

Finally, with the aim to find a good correlation between tortuosity and an appropriate geometrical parameter allowing a relatively easy calculation, we defined an *effective porosity* as the subtraction of the minimum porosity from the nominal one, providing an empirical correlation for tortuosity valid within a relatively wide range of values (0.15–1) usable with a maximum error of 10%.

The presented analysis allows a more precise characterisation of catalytic structures and membranes, putting in evidence hidden aspects relating morphology with surface area and connectivity and contributing in describing more effectively kinetic and transport phenomena involved in membranes and porous media.

Acknowledgements

A. Caravella has received funding through the "Programma Per Giovani Ricercatori "Rita Levi Montalcini" granted by the "Ministero dell'Istruzione, dell'Università e della Ricerca, MIUR" (Grant no. PGR12BV33A), which is gratefully acknowledged.

Authors contributions

G. Azzato and A. Caravella wrote the paper, ran simulations and performed data analysis. G. De Marco contributed to the computational settings for the solution of the diffusion problem. V. Stellato contributed to the structures construction and data analysis. Y. Sun contributed to data analysis and Morphology Map development. A. Caravella developed the main ideas behind the paper, supervised whole manuscript preparation as well as data acquisition.

References

Sunagawa, I., 1999. Growth and morphology of crystals Link: Forma 14, 147–166 www.scipress.org/journals/forma/pdf/1401/14010147.pdf.

Gao, H.Y., He, Y.H., Zou, J., Xu, N.P., Liu, C.T., 2012. Tortuosity factor for porous FeAl intermetallics fabricated by reactive synthesis. Trans. Nonferrous Met. Soc. China (English Ed.) 22, 2179–2183. https://doi.org/10.1016/S1003-6326(11)61446-5.

Schneemann, A., Bon, V., Schwedler, I., Senkovska, I., Kaskel, S., Fischer, R.A., 2014. Flexible metal-organic frameworks. Chem. Soc. Rev. 43, 6062–6096. https://doi.org/10.1039/C4CS00101J.

Pisani, L., 2011. Simple expression for the tortuosity of porous media. Transp. Porous Media 88, 193–203. https://doi.org/10.1007/s11242-011-9734-9.

Zalc, J.M., Reyes, S.C., Iglesia, E., 2004. The effects of diffusion mechanism and void structure on transport rates and tortuosity factors in complex porous structures. Chem. Eng. Sci. 59, 2947–2960. https://doi.org/10.1016/j.ces.2004.04.028.

Caravella, A., Hara, S., Hara, N., Obuchi, A., Uchisawa, J., 2012. Three-dimensional modeling and simulation of a micrometer-sized particle hierarchical structure with macro- and meso-pores. Chem. Eng. J. 210, 363–373. https://doi.org/10.1016/j.cej.2012.08.101.

Caravella, A., Zito, P.F., Brunetti, A., Drioli, E., Barbieri, G., 2016. A novel modelling approach to surface and Knudsen multicomponent diffusion through NaY zeolite membranes. Microporous Mesoporous Mater. 235, 87–99. https://doi.org/10.1016/j.micromeso.2016.07.049.

Delarue, A., Jeulin, D., 2003. 3D morphological analysis of composite materials with aggregates of spherical inclusions. Image Anal Stereol. 22, 153–161. https://doi.org/10.5566/ias.v22.p153-161.

Coleman, S.W., Vassilicos, J.C., 2008. Tortuosity of unsaturated porous fractal materials. Phys. Rev. E - Stat. Nonlinear, Soft Matter Phys. 78, 1–24. https://doi.org/10.1103/PhysRevE.78.016308.

Wiedenmann, D., Keller, L., Holzer, L., Stojadinovic, J., Munch, B., Suarez, L., Fumey, B., Hagendorfer, H., Bronnimann, R., Modregger, P., Gorbar, M., Vogt, U.F., Zuttel, A., La Mantia, F., Wepf, R., Grobety, B., 2013. Three-dimensional pore structure and ion conductivity of porous ceramic diaphragms. AIChE J. 59, 1446–1457. https://doi.org/10.1002/aic.14094.

Moh'd, B.K., 2015. Deriving the pore structure of selected Jordanian building limestones. Jordan J. Earth Environ. Sci. 7, 71–75.

Landesfeind, J., Hattendorff, J., Ehrl, A., Wall, W.A., Gasteiger, H.A., 2016. Tortuosity determination of battery electrodes and separators by impedance spectroscopy. J. Electrochem. Soc. 163, A1373–A1387. https://doi.org/10.1149/2.1141607jes.

Herremans, E., Verboven, P., Verlinden, B.E., Cantre, D., Abera, M., Wevers, M., Nicolaï, B.M., 2015. Automatic analysis of the 3-D microstructure of fruit parenchyma tissue using X-ray micro-CT explains differences in aeration. BMC Plant Biol. 15, 264–277. https://doi.org/10.1186/s12870-015-0650-y.

Grisan, E., Foracchia, M., Ruggeri, A., 2008. A novel method for the automatic grading of retinal vessel tortuosity. IEEE Trans. Med. Imaging 27, 310–319. https://doi.org/10.1109/TMI.2007.904657.

Maude, R.J., Ahmed, B.W., Rahman, A.H., Rahman, R., Majumder, M.I., Menezes, D.B., Sayeed, A.A., Hughes, L., MacGillivray, T.J., Borooah, S., et al., 2014. Retinal changes in visceral leishmaniasis by retinal photography. BMC Infect. Dis. 14, 527. https://doi.org/10.1186/1471-2334-14-527.

Muraoka, Y., Tsujikawa, A., Kumagai, K., Akagi-Kurashige, Y., Ogino, K., Murakami, T., Miyamoto, K., Yoshimura, N., 2014. Retinal vessel tortuosity associated with central retinal vein occlusion: an optical coherence tomography study on tortuous retinal vessels in crvo. Invest. Ophthalmol. Vis. Sci. 55, 134–141. https://doi.org/10.1167/iovs.13-13201.

Sasongko, M.B., Wong, T.Y., Nguyen, T.T., Cheung, C.Y., Shaw, J.E., Kawasaki, R., Lamoureux, E.L., Wang, J.J., 2015. Retinal vessel tortuosity and its relation to traditional and novel vascular risk markers in persons with diabetes. Curr. Eye Res., 1–7 https://doi.org/10.3109/02713683.2015.1034371.

Annunziata, R., Kheirkhah, A., Aggarwal, S., Hamrah, P., Trucco, E., 2016. A fully automated tortuosity quantification system with application to corneal nerve fibres in confocal microscopy images. Med. Image Anal. 32, 216–232. https://doi.org/10.1016/j.media.2016.04.006.

Shen, L., Chen, Z., 2007. Critical review of the impact of tortuosity on diffusion. Chem. Eng. Sci. 62, 3748–3755. https://doi.org/10.1016/j.ces.2007.03.041.

Caravella, A., Hara, S., Obuchi, A., Uchisawa, J., 2012. Role of the bi-dispersion of particle size on tortuosity in isotropic structures of spherical particles by three-dimensional computer simulation. Chem. Eng. Sci. 84, 351–371. https://doi.org/10.1016/j.ces.2012.08.050.

Anovitz, L.M., Cole, D.R., 2015. Characterization and analysis of porosity and pore structures. Rev. Mineral. Geochem. 80, 61–164. https://doi.org/10.2138/rmg.2015.80.04.

Kong, W., Zhang, Q., Gao, X., Zhang, J., Chen, D., Su, S., 2015. A method for predicting the tortuosity of pore phase in solid oxide fuel cells electrode. Int. J. Electrochem. Sci. 10, 5800–5811. https://doi.org/10.13140/RG.2.1.2914.2243.

Bellini, S., Azzato, G., Grandinetti, M., Stellato, V., De Marco, G., Sun, Y., Caravella, A., 2018. A novel connectivity factor for morphological characterization of membranes and porous media: a simulation study on structures of mono-sized spherical particles. Appl. Sci. 8, 573–589. https://doi.org/10.3390/app8040573.

Matyka, M., Khalili, A., Koza, Z., 2008. Tortuosity-porosity relation in porous media flow. Phys. Rev. E - Stat. Nonlinear, Soft Matter Phys. 78, 1–8. https://doi.org/10.1103/PhysRevE.78.026306.

Duda, A., Koza, Z., Matyka, M., 2011. Hydraulic tortuosity in arbitrary porous media flow. Phys. Rev. E - Stat. Nonlinear, Soft Matter Phys. 84, 1–8. https://doi.org/10.1103/PhysRevE.84.036319.

Wang, P., 2014. Lattice Boltzmann simulation of permeability and tortuosity for flow through dense porous media. Math. Probl. Eng. 2014, 1–7. https://doi.org/10.1155/2014/694350. Article ID 694350.

Espinoza, M., Sundén, B., Andersson, M., Yuan, J., 2015. Analysis of porosity and tortuosity in a 2D selected region of solid oxide fuel cell cathode using the lattice boltzmann method. ECS Trans. 65, 59–73. https://doi.org/10.1149/06501.0059ecst.

Kim, A.S., Chen, H., 2006. Diffusive tortuosity factor of solid and soft cake layers: a random walk simulation approach. J. Membrane Sci. 279, 129–139. https://doi.org/10.1016/j.memsci.2005.11.042.

Alam, P., Byholm, T., Toivakka, M., 2006. Calculating tortuosity in quasi-random anisotropic packings. Nord. Pulp Pap. Res. J. 21, 670–675. https://doi.org/10.3183/NPPRJ-2006-21-05-p670-675.

Promentilla, M.A.B., Sugiyama, T., 2007. Studies on 3D micro-geometry and diffusion tortuosity of cement-based materials using x-ray microtomography. In: Proceedings of the 32nd conference on our world in concrete & structures, 28–29 August 2007, Singapore. Article Online Id: 100032047. Online version: <http://cipremier.com/100032047>.

Yamashita, T., Suzuki, K., Adachi, H., Nishino, S., Tomota, Y., 2009. Effect of microscopic internal structure on sound absorption properties of polyurethane foam by x-ray computed tomography observations. Mater. Trans. 50, 373–380. https://doi.org/10.2320/matertrans.MRA2008207.

Gommes, C.J., Bons, A.J., Blacher, S., Dunsmuir, J.H., Tsou, A.H., 2009. Practical methods for measuring the tortuosity of porous materials from binary or gray-tone tomographic reconstructions. AIChE J. 55, 2000–2012. https://doi.org/10.1002/aic.11812.

Vallavh, R., 2009. Modeling Tortuosity in Fibrous Porous Media using Computational Fluid Dynamics Ph.D. Thesis. North Carolina State University, US.

Rezanezhad, F., Quinton, W.L., Price, J.S., Elrick, D., Elliot, T.R., Heck, R.J., 2009. Examining the effect of pore size distribution and shape on flow through unsaturated peat using 3-D computed tomography. Hydrol. Earth Syst. Sci. Discuss. 6, 3835–3862. https://doi.org/10.5194/hess-13-1993-2009.

Szczepanski, Z., Cieszko, M., Zych, G., 2010. Application of micro computer tomography to identification of pore structure parameters of porous materials nanotechnologies and materials. Nanotechnol. Mater., 90–91

Sobieski, W., Zhang, Q., Liu, C., 2012. Predicting tortuosity for airflow through porous beds consisting of randomly packed spherical particles. Transp. Porous Media 93, 431–451. https://doi.org/10.1007/s11242-012-9961-8.

Solórzano, E., Pardo-Alonso, S., Brabant, L., Vicente, J., Van Hoorebeke, L., Rodríguez-Pérez, M.A., 2013. Computational approaches for tortuosity determination in 3D structures. In: Cnudde, V. (Ed.), Book of Abstracts (Talks) of Tomography of Materials and Structures, Ghent, Belgium, pp. 71–74. Link: <http://hdl.handle.net/1854/LU-4178455>.

Manickam, S.S., Gelb, J., McCutcheon, J.R., 2014. Pore structure characterization of asymmetric membranes: non-destructive characterization of porosity and tortuosity. J. Membrane Sci. 454, 549–554. https://doi.org/10.1016/j.memsci.2013.11.044.

Chen-Wiegart, Y.C.K., Demike, R., Erdonmez, C., Thornton, K., Barnett, S.A., Wang, J., 2014. Tortuosity characterization of 3D microstructure at nano-scale for energy storage and conversion materials. J. Power Sources 249, 349–356. https://doi.org/10.1016/j.jpowsour.2013.10.026.

Berg, C.F., 2014. Permeability description by characteristic length, tortuosity, constriction and porosity. Transp. Porous Media 103, 381–400. https://doi.org/10.1007/s11242-014-0307-6.

Ranachowski, Z., Jozwiak-Niedzwiedzka, D., Ranachowski, P., Dabrowski, M., Kudela Jr., S., Dvorak, T., 2015. The determination of diffusive tortuosity in concrete specimens using X-Ray microtomography. Arch. Metall. Mater. 60, 1115–1119. https://doi.org/10.1515/amm-2015-0140.

Khabbazi, A.E., 2015. Numerical and Analytical Characterization of Transport Properties for Single Phase Flows in Granular Porous Media Ph. D. Thesis. University of Toronto, Canada http://hdl.handle.net/1807/70864.

Farlenkov, A.S., Anan'ev, M.V., 2015. Modeling of a microstructure and calculation of a tortuosity factor for cathodic materials of LSM–YSZ. Chimica Techno Acta 2, 16–27. https://doi.org/10.15826/chimtech.2015.2.1.002.

Pawlowski, S., Nayak, N., Meireles, M., Portugal, C.A.M., Velizarov, S., Crespo, J.G., 2018. CFD modelling of flow patterns, tortuosity and residence time distribution in monolithic porous columns reconstructed from X-ray tomography data. Chem. Eng. J. 350, 757–766. https://doi.org/10.1016/j.cej.2018.06.017.

Vogel, H.J., 1997. Morphological determination of pore connectivity as a function of pore size using serial sections. Eur. Hornal Soil Sci. 48, 365–377. https://doi.org/10.1111/j.1365-2389.1997.tb00203.x.

Vogel, H.J., Roth, K., 1998. A new approach for determining effective soil hydraulic functions. Eur. Hornal Soil Sci. 49, 547–556. https://doi.org/10.1046/j.1365-2389.1998.4940547.x.

Moreau, E., Velde, B., Terribile, F., 1999. Comparison of 2D and 3D images of fractures in a vertisol. Geoderma 92, 55–72. https://doi.org/10.1016/S0016-7061(99)00025-7.

Moldrup, P., Olesen, T., Komatsu, T., Schjonning, P., Rolston, D.E., 2001. Tortuosity, diffusivity, and permeability in the soil liquid and gaseous phases. Soil Sci. Soc. Am. J. 65, 613–623. https://doi.org/10.2136/sssaj2001.653613x.

Promentilla, M.A.B., Sugiyama, T., Hitomi, T., Takeda, N., 2009. Quantification of tortuosity in hardened cement pastes using synchrotron- based X-ray computed microtomography. Cement and Concrete Res. 39, 548–557. https://doi.org/10.1016/j.cemconres.2009.03.005.

Lichtner, A.Z., Jauffrès, D., Roussel, D., Charlot, F., Martin, C.L., Bordia, R.K., 2015. Dispersion, connectivity and tortuosity of hierarchical porosity composite SOFC cathodes prepared by freeze-casting. J. Eur. Ceram. Soc. 35, 585–595. https://doi.org/10.1016/j.jeurceramsoc.2014.09.030.

Melo, L.F., 2005. Biofilm physical structure, internal diffusivity and tortuosity Link Water Sci. Technol. 52, 77–84 https://repositorio-aberto.up.pt/bitstream/10216/257/2/55232.pdf.

Le, L.H., Zhang, C., Ta, D., Lou, E., 2010. Measurement of tortuosity in aluminum foams using airborne ultrasound. Ultrasonics 50, 1–5. https://doi.org/10.1016/j.ultras.2009.07.011.

Nwaizu, C., Zhang, Q., 2015. Characterizing tortuous airflow paths in a grain bulk using smoke visualization. Can. Biosyst. Eng./Le Genie Des Biosyst. Au Canada 57, 313–322. https://doi.org/10.7451/CBE.2015.57.3.13.

Brun, E., Vicente, J., Topin, F., Occelli, R., 2008. From 3D imaging of structures to diffusive properties of anisotropic cellular materials. In: Les Presses de l'ecole des mines. Continuous Models and Discrete Systems 11, Aug 2007, Paris, France. pp. 121–127. Link: <https://hal.archives-ouvertes.fr/hal-00199430/document>.

Whitaker, S., 1977. Simultaneous heat, mass and momentum transfer in porous media: a theory of drying. Adv. Heat Transfer 13, 119–203. https://doi.org/10.1016/S0065-2717(08)70223-5.

Kim, J.H., Ochoa, J.A., Whitaker, S., 1987. Diffusion in anisotropic media. Transp. Porous Media 2, 327–356.

Quintard, M., 1993. Diffusion in isotropic and anisotropic porous systems: three-dimensional calculations. Transp. Porous Media 11, 187–199. https://doi.org/10.1007/BF01059634.

Quintard, M., Whitaker, S., 1993. Transport in ordered and disordered porous media: volume-averaged equations, closure problems and comparison with experiments. Chem. Eng. Sci. 48, 2537–2564. https://doi.org/10.1016/0009-2509(93)80266-S.

Ciesko, M., 2009. Description of anisotropic pore space structure of permeable materials based on Minkowski metric space. Arch. Mech. 61, 425–444. https://doi.org/10.1002/zamm.20000801333.

Guo, P., 2012. Dependency of tortuosity and permeability of porous media on directional distribution of pore voids. Transp. Porous Media. 95, 285–303. https://doi.org/10.1007/s11242-012-0043-8.

Fukai, Y., 1984. Site preference of interstitial hydrogen in metals. J. Less Common Met. 101, 1–16.

Maxwell, J.C., 1881. Treatise on Electricity and Magnetism, vol. I, second ed. Clarendon Press, Oxford, UK. Link: <http://www.aproged.pt/biblioteca/MaxwellI.pdf>.

Neale, G.H., Nader, W.K., 1973. Prediction of transport processes within porous media, diffusive flow processes within a homogeneous swarm of spherical particles. AlChE J. 19, 112–119. https://doi.org/10.1002/aic.690190116.